Available online at www.sciencedirect.com
ScienceDirect
Nuclear Instruments and Methods in Physics Research A 577 (2007) 139–145
NUCLEAR INSTRUMENTS & METHODS IN PHYSICS RESEARCH Section A
www.elsevier.com/locate/nima

Beam interaction measurements with a Retarding Field Analyzer in a high-current high-vacuum positively charged particle accelerator

M. Kireeff Covo[a,c,*], A.W. Molvik[a], A. Friedman[a], J.J. Barnard[a], P.A. Seidl[b], B.G. Logan[b], D. Baca[b], J.L. Vujic[c]

[a]*Lawrence Livermore National Laboratory, Heavy-Ion Fusion Science Virtual National Laboratory, Livermore, CA 94550, USA*
[b]*Ernest Orlando Lawrence Berkeley National Laboratory, Heavy-Ion Fusion Science Virtual National Laboratory, 1 Cyclotron Road, Berkeley, CA 94720, USA*
[c]*University of California at Berkeley, 4155 Etcheverry Hall, MC 1730, Berkeley, CA 94720, USA*

Available online 22 February 2007

Abstract

A Retarding Field Analyzer (RFA) was inserted in a drift region of the magnetic transport section of the High-Current Experiment (HCX), that is at high-vacuum, to measure ions and electrons resulting from beam interaction with background gas and walls. The ions are expelled during the beam pulse by the space–charge potential and the electrons are expelled mainly at the end of the beam, when the beam potential decays. The ion energy distribution shows the beam potential of ~2100 V and the beam–background gas total cross-section of 3.1×10^{-19} m^2. The electron energy distribution reveals that the expelled electrons are mainly desorbed from the walls and gain ~22 eV from the beam potential decaying with time before entering the RFA. Details of the RFA design and of the measured energy distributions are presented and discussed.

PACS: 29.30.Aj; 34.50.Dy; 41.75.Ak; 79.20.Rf

Keywords: Energy analyzer; Diagnostics; Positively charged beam; High-current accelerator; High-vacuum

1. Introduction

The High-Current Experiment (HCX) [1] at Lawrence Berkeley National Laboratory (LBNL) is a 1 MeV linear DC accelerator with K^+ ion beam current of 180 mA for 5 μs that produces a space–charge beam potential of ~2100 V. It is used to develop and apply diagnostics that can identify and quantify sources of electrons, as well as to validate three-dimensional self-consistent WARP simulations of electron cloud effects [2].

Quantitative measurements of beam interaction can be done with a Retarding Field Analyzer (RFA) [3], which constitutes a high-pass energy filter for positive ions or electrons that cross the aperture. The Advanced Photon Source (APS) at ANL used a special vacuum chamber with 10 RFAs and three beam position monitors to measure properties of electron cloud [4], which subsequently was improved with an amplifier and sweeper and used at the Proton Storage Ring (PSR) at LANL [5] and at the KEK-PS [6].

Similar detectors, also based on the RFA from APS, were installed at Beijing Electron Positron Collider (BEPC) in IHEP [7] and at the Low Energy Positron Ring (LER) in KEKB [8].

A RFA was adapted from Rosenberg's design [9], which simplified construction through use of commercial parts, and inserted in the drift region between quadrupole magnets, where the magnetic fringe fields vanish. The design included: an extra grid placed to suppress electrons right after the entrance, which minimizes secondary electrons, electron-induced gas desorption and ionization

*Corresponding author. University of California at Berkeley, 4155 Etcheverry Hall, MC 1730, Berkeley, CA 94720, USA.
Tel./fax: +1 510 540 6473.
E-mail address: kireeffcovo1@llnl.gov (M. Kireeff Covo).

0168-9002/$ - see front matter © 2007 Elsevier B.V. All rights reserved.
doi:10.1016/j.nima.2007.02.045

inside the RFA; large gaps, which hold up to 3 keV; and a compact 5 cm linear motion feedthrough, that allows positioning the RFA.

The modifications allowed ion and electron energy measurements inside a high-current high-vacuum positively charged particle accelerator. Details of the RFA design and a discussion of the experimental results are provided.

2. Beam interaction overview

The beam can interact with the background gas, producing ions and electrons, and the walls, desorbing electrons and gas.

The Gas-Electron Source Diagnostics (GESD) experiment [10] predicts that a 1 MeV K+ ion impact near grazing incidence on stainless steel desorbs ~10,000 molecules of gas and produces ~100 electrons. Those electrons have a cosine distribution to the surface normal and in some conditions can multiply.

The average velocity of gas is 0.5 mm/μs [11], since the beam duration is ~5 μs, the average gas cloud front should not expand into the beam path and consequently will not be directly ionized.

The interaction of the K+ ion with the background gas occurs mainly by two mechanisms:

$$K^+ + g^0 \rightarrow K^+ + g^+ + e^- \text{ (ionization)}$$

$$K^+ + g^0 \rightarrow K^0 + g^+ \text{ (charge exchange)}.$$

Gas ionization is the only process that will produce electrons (e^-) that may be trapped with the same profile of the beam, and expelled at the end of the beam when the electrostatic potential drops down; but both processes (ionization and charge exchange) will produce cold ions (g^+) that will be expelled during the passage of the beam by the beam space-charge potential.

The ions are born with a potential energy that is totally converted into kinetic energy at the moment that they reach the walls or enter the RFA, not exceeding the beam potential. The electrons gain energy as the beam potential decays, reaching the walls or entering the RFA.

3. RFA description

A sketch of the analyzer geometry is presented in Fig. 1. It consists of a grounded box with entrance of 5.1 cm (transverse to the beam) × 4.1 cm (along the beam), which has a sampling orifice made of a 0.1 mm foil to approximate a knife edge with a double-mesh gridded aperture of 0.5 cm × 1.5 cm. A double-mesh grid is an arrangement where two consecutive grids are held together separated by more than a mesh opening to assure the potential between them.

The entrance is followed by three single grids of 2.5 cm × 2.5 cm and a collector, separated by gaps of $d1 = 0.8$ cm, $d2 = 1$ cm, $d3 = 0.8$ cm and $d4 = 0.8$ cm. All grids are made of woven 304 stainless steel with 20 mesh/cm and a transparency of 88%. The grids are spot welded on 2.5 cm × 2.5 cm × 0.6 mm stainless steel frames that are electrically insulated by alumina spacers.

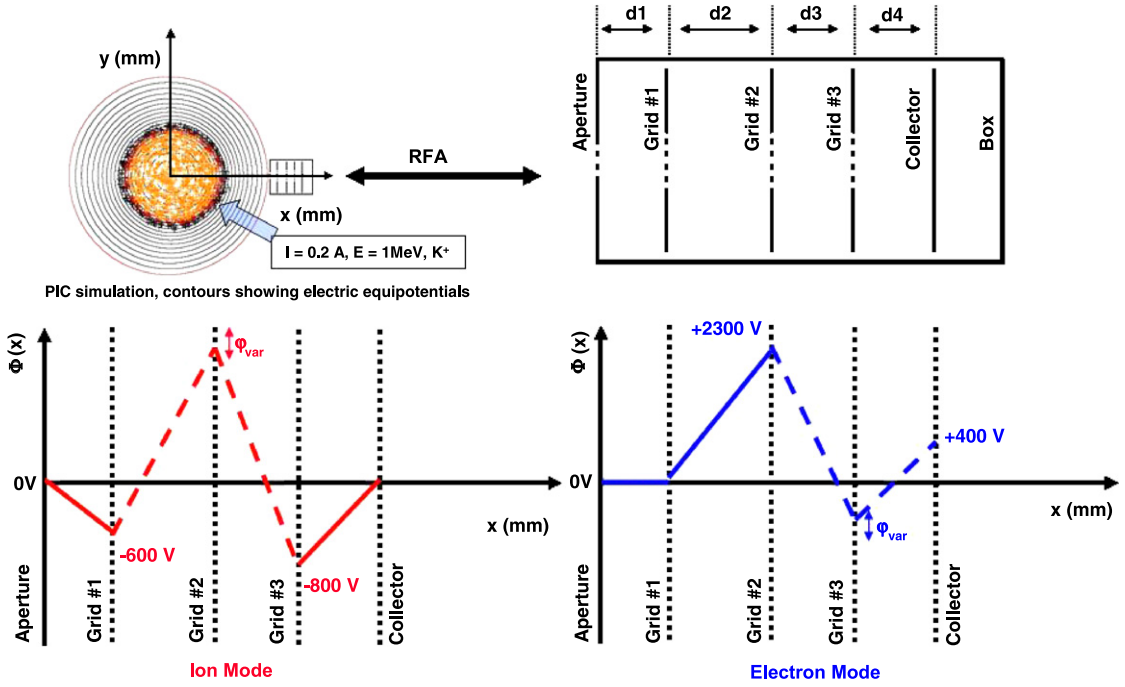

Fig. 1. (Color online) Sketch of the analyzer geometry that is placed at 4 cm of the beam center. It has an aperture, three grids and a collector, and can work in either the ion or electron modes. The ion mode uses biases in red color shown at the lower left; it suppresses electrons immediately after the entrance, and energy-filters ions entering the RFA. The electron mode uses biases in blue color shown at lower right; it suppresses ions, and energy-filters electrons entering the RFA.

The actual grid transparency differs from the optical and varies with the retarding field [12]. The transparency used in this work will be assumed constant and equal to the optical, giving a total grid transmission of 53%.

Only particles entering on trajectories nearly parallel to the x direction (RFA normal) can reach the collector. The aperture geometry will minimize halo from reaching the collector and the alumina spacers.

The collector is 3.3 cm from the aperture and is coated with Aquadag^{TM} to decrease the number of secondary electrons. A charge sensitive preamplifier is connected to the collector, using a double shielded cable to reduce noise. The preamplifier, which has a gain of up to 1.4 V/pC, can integrate a small burst of current, producing an output that is proportional to the total charge collected with a decay time of 140 μs.

The RFA entrance is placed at 4 cm from the center of the beam and is mounted on a compact 5 cm linear motion feedthrough to allow radial motion. At a radius of 4 cm the beam space-charge equipotential (obtained using a three-dimensional self-consistent WARP code simulation) is near 0 V, matching the potential of the analyzer box, which is grounded.

The RFA operates as a high-pass energy filter for either positive ions or electrons entering the aperture, designated ion or electron modes, respectively. The lower left grid biases in red they are used to measure the energy distribution of positive ions (ion mode). The lower right grid biases in blue they are used to measure the energy distribution of electrons (electron mode).

In order to infer the total ion or electron charge over the length of the entrance grid, the charge intensity measured in either mode needs to be divided by the total grid transmission of 53% and multiplied by 49.5 to correct for the angle subtended by the RFA aperture as viewed by the center of the beam, which corresponds to 7.3°.

The HCX facility is at high-vacuum with a background pressure inside the magnets of $\sim 4.6 \times 10^{-7}$ Torr. Assuming a total collision cross-section of 10^{-18} m^2, a mean free path of 66 m is obtained, so collisions of expelled ions or electrons in the way of the RFA are discarded.

3.1. Ion mode

If the RFA is in its ion mode, grid No. 1 (Fig. 1) is biased to −600 V to repel incoming electrons that are expelled mainly at the end of the beam, when the beam potential drops down. This large flux of electrons entering the RFA must be suppressed near the aperture to avoid spurious signals generated inside the analyzer, coming from secondary electrons, as well as electron-induced gas desorption and ionization.

The retarding potential in grid No. 2 varies from 0 to 2300 V. The grid is an energy filter, allowing only particles with energy E in the x direction greater than qV to overcome the potential barrier, where q is the charge from the particle and V is the potential applied to the retarding grid No. 2.

Grid No. 3 is biased either to repel electrons from the collector and from all the other grids and supports.

The ion-induced electrons from the collector will be emitted by potential electron emission mechanism [13], which gives a maximum energy of $E_i - 2\Phi$, where E_i denotes the ionization energy from incident ion and Φ the work function from a target. The work function from the graphite-coated collector is 4.5 eV and for most of the single ion species the ionization potential will be less than 15 eV, giving the maximum energy for an ion-induced electron of only ~6 eV.

The grid No. 3 bias must be more negative than the bias applied to grid No. 1 in order to suppress particle-induced electrons from grid No. 1 penetrating beyond grid No. 3. This procedure also prevents secondary electrons from being trapped between the suppressors. The bias choice of −800 V should suppress most of the auger electrons from excited atoms, which have less than 800 eV [14].

The filtered ion current will reach the grounded collector and be integrated by the charge sensitive preamplifier. The procedure to acquire the ion energy distribution consists of taking measurements varying the retarding grid No. 2 bias from shot to shot. Ions will originate from both ionization of gas as well as charge exchange with the beam.

The present apparatus configuration cannot distinguish single and double ionization or ion species, because we do not perform the ion energy distribution in series with a mass filter. However, a measurement of background gas components with a residual gas analyzer (RGA) obtained mainly H_2O, followed by H_2 and N_2. It implies that a 1 keV H_2O^+ ion will reach the wall or enter the RFA in 389 ns, or faster if the ion species is lighter.

3.2. Electron mode

If the RFA is in its electron mode, grid No. 2 is biased to +2300 V to repel incoming ions from background gas ionization and charge exchange that are expelled during the beam pulse.

Electrons are filtered depending on their kinetic energy in x direction by a retarding potential in grid No. 3 that varies from 0 to −400 V. An intrinsic problem arises when the grid No. 3 bias is close to 0 V, because it will not suppress particle-induced electrons generated inside the analyzer.

The filtered electrons will reach the collector that is biased to +400 V and be integrated by the charge sensitive preamplifier. It is important to bias the collector positively enough to suppress its own particle-induced electrons that otherwise would combine with the signal measured.

A similar procedure to the previous section is used to acquire the electron energy distribution by changing the bias of grid No. 3 from shot to shot.

4. Energy resolution

The analyzer energy resolution is defined as the ratio $\Delta E/E$, where ΔE is a decrease of the component of the ion

kinetic energy E parallel to the analyzer x axis (Fig. 1) caused by a deviation in the ion trajectory before being filtered.

A planar RFA retards the incident particles only in the direction normal to the grids. The resolution is function of angle of incidence of the particle and is given by [15]:

$$\left(\frac{\Delta E}{E}\right)_{\text{shift}} = \sin^2(\theta)$$

where θ is the incidence angle from the ion. If the RFA is placed at 4 cm from the center and we assume that the ions are expelled radially we obtain ~0.4%.

This error may be eliminated if a nested cylindrical grid or a conical aperture is used to change the electric field lines within the RFA [16].

Another source of energy analysis error is given by lens effects, because stronger fields always penetrate in the region of weaker fields, i.e., the equipotential lines tend to penetrate between the wires from the retarding grid and form convex surfaces towards the weaker fields [17]. The magnitude of this error is given by [18]:

$$\left(\frac{\Delta E}{E}\right)_{\text{width}} = 1 - \frac{2\pi(d/a) - \ln(4)}{2\pi(d/a) - 2\,\ln[2\sin(\pi r/a)]}$$

where d is the distance between grids, a is the distance between wires and r is the wire radius. The RFA grids have $d/a \sim 169$ and $r/a \sim 0.06$, giving ~0.3% of error.

This error may be minimized by employing multiple grids, giving a more uniform potential in the center of the retarding potential, or by increasing d/a, using fine meshes or enlarging the distance between grids [19].

If the errors add in quadrature, the total RFA resolution obtained is 0.5%.

5. Particle suppression

In the ion mode we prevent electrons from reaching the collector, likewise in the electron mode we prevent ions. The Debye length (λ_D) will be a critical parameter for the correct analyzer operation and is given by [20]:

$$\lambda_D = \left(\frac{\varepsilon_0 \kappa_B T}{ne^2}\right)^{1/2}$$

where ε_0, K_B, T, n and e denote the dielectric constant, the Boltzman constant, the mean temperature, the density and the elementary charge, respectively.

In order to effectively suppress ions (electron mode) or electrons (ion mode), the "grid hole radius" condition $a/2$ ($\sim 1.4 \times 10^{-4}$ m) $< \lambda_D$ must be satisfied [21]. Electrons from different sources accumulate during the beam passage, being expelled at the end of the beam. From the Faraday cup data, it can be inferred a beam potential decay rate of ~1600 V/μs, so, for an electron bounce time of 20 ns, an electron at rest near the opposite wall will gain 32 eV before entering the RFA. Assuming that 32 eV represents the mean electron temperature and that the electron density is in the order of the beam density, the Debye length for electrons expelled at the end of the beam is 4.4×10^{-3} m.

The HCX operates at $\sim 5 \times 10^{-7}$ Torr with potential of ~2000 V; assuming conservatively a beam–background interaction total cross-section of 10^{-19} m^2 and mean ion temperature of 1000 eV (half of the beam potential), the ion density of 5.6×10^{11} m^{-3} is obtained, which gives a Debye length for ions expelled during the beam pulse of 3.1×10^{-1} m.

The results are summarized in Table 1 and satisfy the "grid hole radius" condition.

6. Space–charge limits

The ions and electrons going inside the RFA must not exceed the Child–Langmuir density to avoid being space–charge current limited. The Child–Langmuir law states that [22,23]:

$$j(\text{A/cm}^2) = \frac{\varepsilon_0}{9\pi}\left(\frac{2e}{m}\right)^{1/2}\frac{V^{3/2}}{d^2}$$

where ε_0, e, V, m and d denote the vacuum permittivity, the elementary charge, the bias potential between planar parallel electrodes, the particle mass and the distance between the electrodes, respectively.

For the ions case, assuming a beam–background interaction total cross-section of 10^{-19} m^2, beam current of 180 mA and background pressure of 5×10^{-7} Torr, at room temperature the ion current density at the RFA entrance is $\sim 1.2 \times 10^{-3}$ A/m^2. In the worst-case scenario, for an expelled ion of 40 AMU and using the bias solution and dimensions from Fig. 1, the Child–Langmuir law gives an upper limit of ~1.8 A/m^2.

For the electrons case, as the electrons are trapped and expelled at the end of the beam, conservatively assuming an electron density of 10^{14} m^{-3} (~beam density) and a mean electron temperature of 32 eV, the electron current density is ~5.5 A/m^2. For expelled electrons, using the bias solution and dimensions from Fig. 1, the Child–Langmuir law gives an upper limit of $\sim 3.2 \times 10^2$ A/m^2.

Table 1
Debye length for expelled ions and electrons compared with grid hole radius

Debye length for electrons (m)	Debye length for ions (m)	Grid hole radius (m)
$\sim 4.4 \times 10^{-3}$	$\sim 3.1 \times 10^{-1}$	$\sim 1.4 \times 10^{-4}$

Table 2
Current density for expelled ions and electrons compared with Child–Langmuir (CL) space current density limit

Ions		Electrons	
Current density (A/m^2)	CL limit (A/m^2)	Current density (A/m^2)	CL limit (A/m^2)
$\sim 1.2 \times 10^{-3}$	~1.8	~5.5	$\sim 3.2 \times 10^2$

The results are summarized in Table 2 and satisfy the Child–Langmuir law.

7. Experimental results

7.1. Ion mode

The ions produced from ionization and charge exchange beam interaction with background gas are expelled during the beam passage by the beam potential.

Fig. 2(a) shows the charge collected raw data, obtained with the RFA working in ion mode, after subtraction of a low frequency background noise of ~786 Hz that is superposed to the collector signal. The raw data uses the right-hand ordinate axis and the legend at the right side shows the retarding grid bias applied. The Faraday cup current (FC) uses the left-hand ordinate axis and is corrected for the time-of-flight from the beam. The vertical red line at 4.5 μs shows the moment that the ion energy distribution, plotted in Fig. 2(b), is measured.

The ion potential energy, given by the place where the ion was born, is totally converted in kinetic energy at the entrance of the RFA; as a result the beam potential corresponds to the moment that the RFA; collector does not measure more charge, i.e., at ~2100 V. The RFA is a high-pass energy filter, therefore the beam edge potential is the place where the charge collected starts to decrease steeply, i.e., at ~1000 V. The beam halo is between 0 V and the beam edge, corresponding to the place where the ion energy distribution flattens out.

7.2. Electron mode

There are two sources of trapped electrons: electrons desorbed from walls and from ionization of background gas.

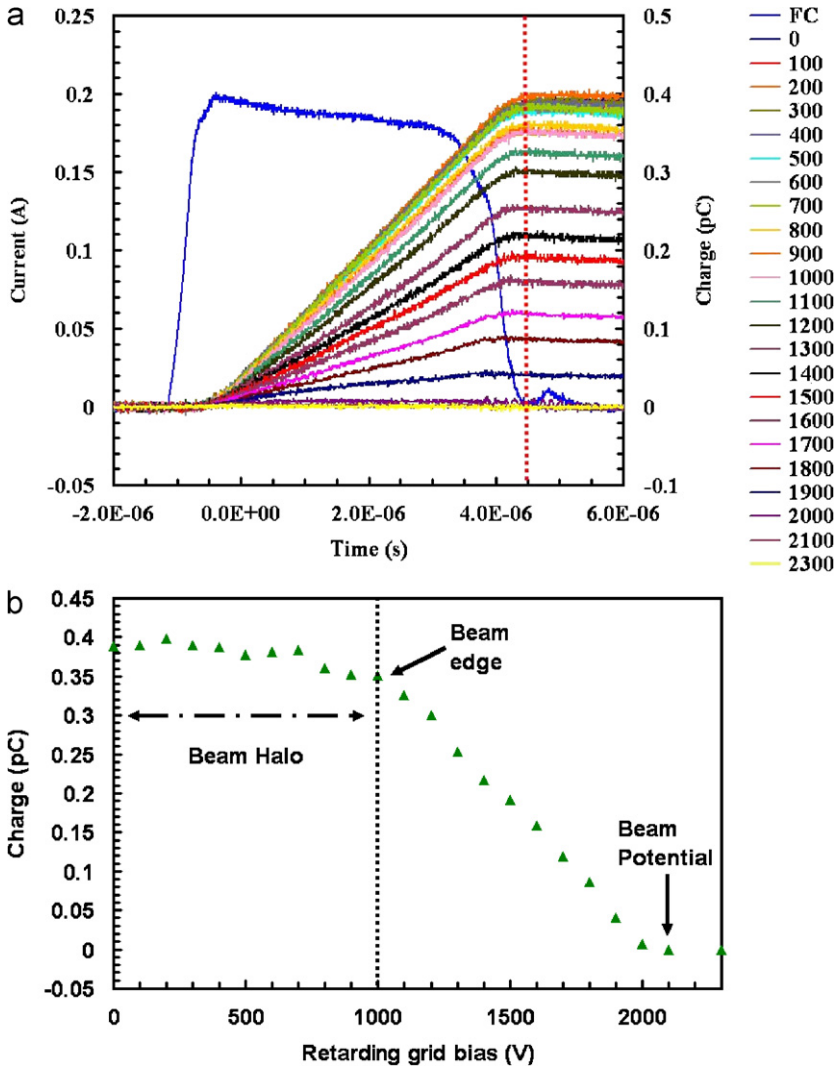

Fig. 2. (Color online) (a) From the top of the legend to the bottom are: the Faraday cup corrected for the time-of-flight; and the raw data signal for RFA working in its ion mode with grid No. 2 bias varying between 0 and 2300 V. (b) Expelled ion energy distribution obtained at 4.5 μs (vertical dashed red line from (a)), when the RFA is working in its ion mode. It has the information of the beam potential, the beam edge potential, and beam halo distribution measured.

Electrons originated from walls can be trapped at the beginning of the beam, when the beam potential that is rising up at a rate of 2000 V/μs overcomes the electron energy.

All the cold electrons from the background and desorbed gas ionization are produced inside the beam pipe and will not overcome the potential energy needed to reach the wall. The trapped electrons will accumulate and be expelled at the end of the beam when the beam potential decays.

Fig. 3(a) shows several RFA collector signals in the electron mode plotted using right-hand ordinate axis and the Faraday cup current (FC) plotted using left-hand ordinate axis. The electron retarding grid biases are listed in the side legend.

The beam potential drops down at a rate of ~1600 V/μs; assuming an electron bounce time of 20 ns and that the electrons start at rest from the opposite diameter end to the RFA, the electrons gain 32 eV before entering the RFA. It is in fair agreement with the data from Fig. 3(b), which shows no electrons with less than 22 eV.

The total electron charge measured is ~ -26 pC and corresponds to 65 times the total ion charge measured, which corresponds to an upper limit of beam–background gas ionization if the charge exchange is neglected.

A problem arises from this measurement, because at the same time that the trapped electrons are expelled, the beam tail scrapes the wall producing electrons. The created ion-induced electrons will also gain energy given from the beam potential dropping, being indistinguishable from those trapped and contributing to the signal measured. These electrons will add up to the signal misleading absolute measurements of trapped electrons.

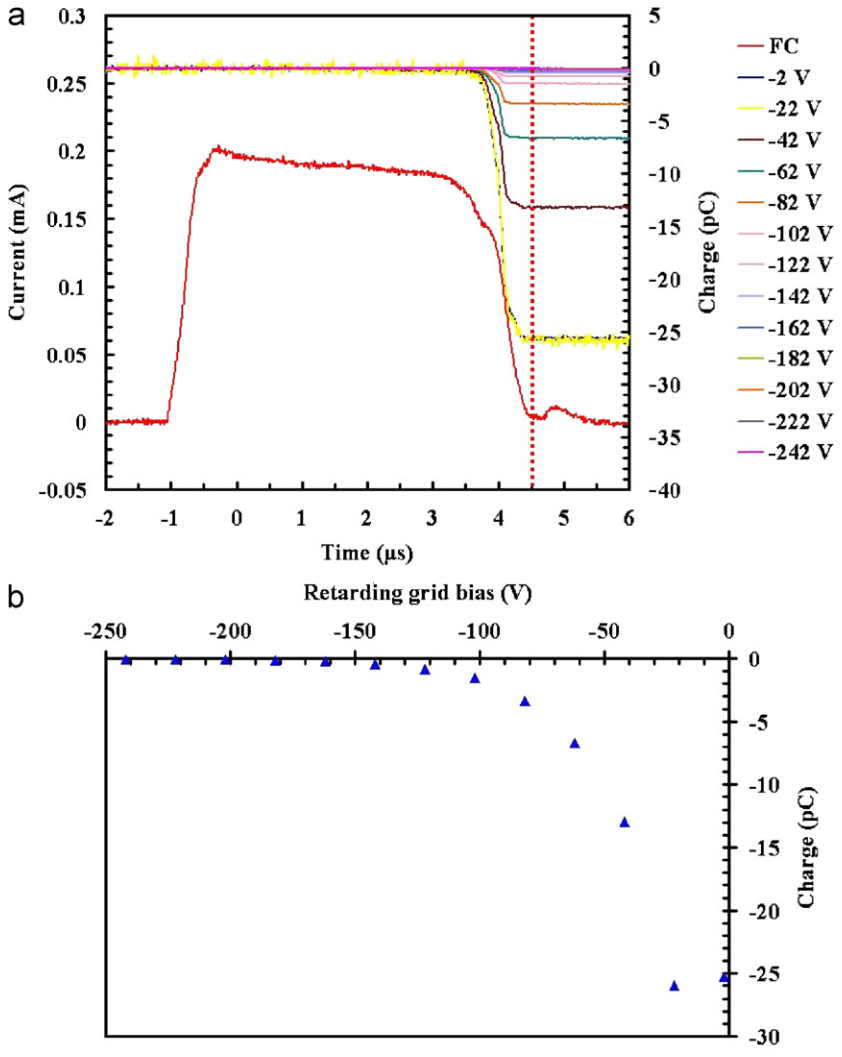

Fig. 3. (Color online) (a) From the top of the legend to the bottom are: the Faraday cup corrected for the time-of-flight; and the raw data signal for RFA working in its electron mode with grid No. 3 bias varying between −2 and −242 V. (b) Expelled electron energy distribution obtained at 4.5 μs (vertical dashed red line from (a)), when the RFA is working in its electron mode. It shows that electrons expelled at the end of the beam are mainly from the walls and have low energy.

8. Conclusions

The beam can interact with the background gas and produce ions and electrons. The ions will be expelled during the beam passage and the electrons will be trapped and expelled at the end of the beam, when the beam potential decays.

The beam can also interact with the walls and desorb gas and electrons. As the average velocity of gas is 0.5 mm/μs, the desorbed gas will not be directly ionized. The desorbed electrons will be trapped at the beginning of the beam, when the beam potential is rising up. The beam tail scrapes the wall and produces electrons, which will add up to the trapped electrons that are expelled at the end of the beam.

A RFA is designed to measure the ions and electrons from beam interaction inside the HCX. The RFA grids provide particle suppression and do not space–charge limit the expelled particle current. The RFA has final energy resolution of 0.5% and measures a total charge collected in Figs. 2(b) and 3(b) of 0.4 and −26 pC, respectively. Assuming that all ions entering the RFA will be mainly single ionized, the beam–background total cross-section is $3.1 \times 10^{-19}\,m^2$. The upper limit for electrons produced from ionization is given by 0.4 pC (discarding charge exchange), which provides a maximum electron line charge of $2.5 \times 10^{-9}\,C/m$, that corresponds to ~3% of the beam line charge, meaning that the main source of electrons at the end of the beam is not from background gas ionization, but from the walls.

Fig. 2(b) gives a beam potential of ~2100 V and a beam edge potential of ~1000 V. Fig. 3(b) also shows that the low energetic electrons expelled at the end of the beam gain ~22 eV from the beam potential decaying with time.

The measurements show that the RFA works either in the ion and electron modes and is suitable for measurements inside a high-current high-vacuum positively charged particle accelerator, where a large amount of electrons accumulate and are expelled at the end of the beam.

Acknowledgments

We wish to thank Tak Katayanagi who built the RFA, Wayne G. Greenway, Larry W. Mills and Gary Ritchie who maintain HCX, and Craig Rogers, Ed Romero and William L. Waldron who provided electronic support. We also want to express our gratitude to Richard A. Rosenberg and Katherine C. Harkay for sharing details that aided our RFA design, and to Miguel Furman for his insightful comments. This work was performed under the auspices of U.S. Department of Energy by the University of California, LLNL and LBNL under contracts No. W-7405-ENG-48, and No. DE-AC02-05CH11231.

References

[1] L.R. Prost, F.M. Bieniosek, C.M. Celata, C.C. Dugan, A. Faltens, P.A. Seidl, W.L. Waldron, R. Cohen, A. Friedman, M. Kireeff Covo, S.M. Lund, A.W. Molvik, Nucl. Instr. and Meth. A 544 (2005) 151.
[2] R.H. Cohen, A. Friedman, S.M. Lund, A.W. Molvik, T. Azevedo, J.-L. Vay, P. Stoltz, S. Veitzer, Nucl. Instr. and Meth. A 544 (2005) 210.
[3] R.A. Pitts, R. Chavan, S.J. Davies, S.K. Erents, G. Kaveney, G.F. Vince, JET-EFDA workprogramme Contributors, I. Duran, Rev. Sci. Instr. 74 (2003) 4644.
[4] K.C. Harkay, R.A. Rosenberg, in: Proceedings of the Particle Accelerator Conference IEEE, New York, NY, 1999, p. 1641.
[5] R.J. Macek, A. Browman, M. Borden, D. Fitzgerald, T.S. Wang, T. Zaugg, K.C. Harkay, R.A. Rosenberg, in: Proceedings of the Particle Accelerator Conference IEEE, Portland, OR, 2003, p. 508.
[6] T. Toyama, in: Proceedings of ECLOUD04, Napa, CA, 2004, ⟨http://mafurman.lbl.gov/ECLOUD04_proceedings/toyama_ECLOUD04_v4.pdf⟩.
[7] Z.W. Guo, Q. Qin, J.S. Cao, H. Huang, L. Ma, J.Q. Wang, J. Xing, G. Xu, C. Zhang, Z. Zhao, K.C. Harkay, H. Fukuma, E. Kikutani, M. Tejima, in: Proceedings of the Second Particle Accelerator Conference, Beijing, China, 2001, p. 377.
[8] K. Kanazawa, H. Hukuma, H. Hisamatsu, Y. Suetsugu, in: Proceedings of the Particle Accelerator Conference, Knoxville, TN, 2005, p. 1054.
[9] R.A. Rosenberg, K. Harkay, Nucl. Instr. and Meth. A 453 (2000) 507.
[10] A.W. Molvik, M. Kireeff Covo, F.M. Bieniosek, L. Prost, P. Seidl, D. Baca, A. Coorey, A. Sakumi, Phys. Rev. ST Accel. Beams 7 (2004) 093202.
[11] F.M. Bieniosek, Phys. Rev. ST Accel. Beams, to be published.
[12] P. Nenovski, I. Kutiev, M. Karadimov, J. Phys. E 13 (1980) 1011.
[13] R.A. Baragiola, Nucl. Instr. and Meth. B 78 (1993) 223.
[14] K. Oura, V.G. Lifshits, A.A. Saranin, A.V. Zotov, M. Katayama, Surface Science: An Introduction, Springer, Berlin, 2003, p. 86.
[15] J.A. Simpson, Rev. Sci. Instrum. 32 (1961) 1283.
[16] C.L. Enloe, Rev. Sci. Instrum. 65 (1994) 507.
[17] O. Klemperer, Electron Physics, Butterworths, London, 1959, pp. 41–43.
[18] K.R. Spangenberg, Vacuum Tubes, McGraw-Hill, New York, 1948, p. 279.
[19] C.L. Enloe, J.R. Shell, Rev. Sci. Instrum. 63 (1992) 1788.
[20] C. Böhm, J. Perrin, Rev. Sci. Instrum. 64 (1993) 31.
[21] A.W. Molvik, Rev. Sci. Instrum. 52 (1981) 704.
[22] C.D. Child, Phys. Rev. 32 (1911) 492.
[23] I. Langmuir, Phys. Rev. 21 (1921) 419.